Polymer 154 (2018) 241–252

Contents lists available at ScienceDirect

Polymer

journal homepage: www.elsevier.com/locate/polymer

# Tailoring the mechanical, thermal, and flammability properties of high-performance PEI/PBT blends exhibiting dual-phase continuity

Mauricio Vásquez-Rendón[a,b,*], Mónica Lucía Álvarez-Láinez[a]

[a] Grupo de Investigación en Ingeniería de Diseño, Universidad EAFIT, Carrera 49 # 9sur-50, Medellín, Antioquia, Colombia
[b] Instituto Tecnológico Metropolitano, ITM, Campus Robledo, Calle 73 No. 76A-354, Medellín, Antioquia, Colombia

## HIGHLIGHTS

- New evidences of PEI/PBT blends immiscibility are shown.
- Morphological evolution is described in the entire compositional range.
- A new spore-like morphology is introduced.
- Mechanical, thermal, and flammability performance strongly depends on morphology.
- PEI improves thermal and flame resistance of PBT and enhances charring formation.

## ARTICLE INFO

*Keywords:*
High-performance polymer blends (HPPB)
PEI
PBT
Partially miscible blends
Dual-phase continuity
Tailored morphology

## ABSTRACT

Binary PEI/PBT blends are prepared using a two-step melt processing method. Miscibility study by MDSC and DMA reveals partial miscibility, and new evidence on the morphological evolution of PEI/PBT blends is presented. Two groups of blends are recognized: PBT-rich blends and PEI-rich blends, as well as phase inversion at concentrations close to 50 wt% of PEI. Mechanical, thermal, and flame resistance performance is influenced by blends morphology, and an opportunity for tailoring blends properties is recognized. Tensile modulus shows synergic contribution for 50/50 and 80/20 blends and yield strength is strongly affected by interfacial adherence between constituents. In addition, elongation at break is compromised by PBT-rich blends morphology, and by PEI-rich blends densification. The 50/50 blend exhibits the best elongational at break result due to its co-continuous morphology. Thermal stability and flammability tests reveal that PEI improves the thermal resistance and charring of PBT, particularly for 50/50 blend.

## 1. Introduction

Fabrication of protective elements for automotive, aerospace, electrical and fire protection industries require applying light materials with outstanding mechanical, thermal, and fire resistance performance. However, commonly used materials such as poly(benzimidazole) (PBI), poly(phenylene sulphide) (PPS), poly(vinyl chloride) (PVC), and mod-acrylic, lack all these properties by themselves [1]. Fabrication of high-performance polymer blends (HPPB) appears as an attractive opportunity to obtain materials that combine superior properties with good melt processability [2,3]. The high-performance polymers (HPP) family comprises three main groups: engineering, specialty, and ultra-high performance polymers [4]. Engineering polymers exhibit high mechanical performance and good processability. However, they cannot be used in demanding applications that require continuous use temperatures (CUT) higher than 140 °C. This group mainly involves poly(amides) (PA), poly(carbonates) (PC), poly(esters) (PBT, PET, PTT), and poly(acetal) (POM). On the other hand, specialty and ultra-high performance polymers, such as poly(fluoro carbons) (PTFE, PVDF), sulfur-containing polymers (PPS), poly(imides) (PI, PEI), and poly(ether ketones) (PEEK), have excellent mechanical properties and thermal stability, and some of them display inherent flame resistance with CUT that can reach up to 240 °C [2,5,6]. However, it is difficult to work with these polymers due to their poor melt processability and high costs. Despite the expected benefits of combining HPP in a single material, most efforts in blending technology are focused on the production of commodity polymer blends [7–12].

Blending poly(ether imide) (PEI) with poly(butylene terephthalate) (PBT) is a good example of combining high-performance materials with good processability. PEI is an amorphous specialty polymer with high

* Corresponding author. Instituto Tecnológico Metropolitano, ITM, Campus Robledo, Calle 73 No. 76A-354, Medellín, Antioquia, Colombia.
*E-mail address:* mvasqu27@eafit.edu.co (M. Vásquez-Rendón).

https://doi.org/10.1016/j.polymer.2018.09.012
Received 22 June 2018; Received in revised form 4 September 2018; Accepted 7 September 2018
Available online 11 September 2018
0032-3861/ 

glass transition temperature (Tg) (~216 °C), exceptional mechanical properties, thermal stability, and inherent flame resistance; while PBT is a semicrystalline engineering polymer with low Tg (~50 °C), outstanding chemical resistance and mechanical strength. Blends between PEI and PBT have been studied by different processing techniques including melt processing [13–17]. These authors described complete miscibility within the entire compositional range by means of DSC, DMA, or FTIR analyses, regardless the blending method used: solution or melt blending. Some of these works, evaluated miscibility by thermal analysis and found that Tg and cold crystallization temperature (Tcc) of PBT shifted to higher temperatures as a consequence of increasing chains stiffness during PEI addition [14–16]. Woo [14] complemented the thermal analysis results with optical microscopy and SEM observations, finding transparent and homogeneous phases. However, the morphological evaluation presented lacks clear evidence of phase differences between PEI and PBT, and it is not possible to conclude if these polymers are truly miscible.

In this work, we develop high-performance PEI/PBT blends within the entire compositional range using the two-step processing method described in our previous work [18], and approach a miscibility study by thermal analysis using modulated differential scanning calorimetry (MDSC) and dynamic mechanical analysis (DMA). We track the Tg of both components, since a single Tg is the most widely accepted criteria for miscibility [19–23]. Miscibility results are compared to structure and morphological evolution study in the entire compositional range by using Soxhlet selective extraction technique together with SEM and TEM. In addition, we report for the first time the effects of miscibility and morphology on the mechanical, thermal stability and flammability behavior of PEI/PBT blends, and identify an opportunity to control their morphology in order to tailor the properties for specific high-performance applications.

## 2. Experimental

### 2.1. Materials and blends fabrication

Two commercial grade polymers were purchased from Sabic Innovative Plastics: poly(ether imide) (PEI) Ultem 1000, and poly(butylene terephthalate) (PBT) filled with a flame retardant additive (brominated and antimony trioxide compound) Valox 310SE0. Binary blends between PEI and flame retarded PBT were prepared in an internal mixer by using the two-step processing method described in our previous work [18]. Blends were designated as PEI/PBT according to the weight percentage, and two groups of blends: PBT-rich blends (< 50 wt% of PEI) and PEI rich blends (> 50 wt% of PEI) were differentiated.

### 2.2. Miscibility study

Tg of both components were tracked using modulated differential scanning calorimetry (MDSC) and dynamic mechanical analysis (DMA). MDSC tests were performed in a DSC Q200 from TA Instruments. Samples of 20±1 mg were set up from 0 °C to 290 °C at 20 °C/min, followed by cooling to −30 °C at 20 °C/min, and a second heating was made in modulated mode up to 300 °C at 2 °C/min with an amplitude of ±1.27 and a period of 60 s.

DMA experiments were completed under torsional mode using the solid clamps assembly of a HAAKE MARS III rheometer from Thermo Scientific. Injected molded samples were obtained in a HAAKE MiniJet Pro Injection System from Thermo Scientific using a cylinder temperature from 270 °C to 360 °C, molding temperature of 120 °C, injection pressure from 400 bar to 550 bar with a holding time of 6 s, and post pressure from 300 bar to 550 bar with a holding time from 2 s to 6 s. A complete description of injection parameters for each blend is presented in the Supplementary Material Section. Samples were cut up to 8 × 10 × 4 ± 0.2 mm and heated from 30 °C to 250 °C at 5 °C/min. A frequency of 1 Hz and strain of 0.5% were used to ensure the linear viscoelastic region. Samples were preconditioned before testing within a strain program from 0.1% to 1.2% at 30 °C.

### 2.3. Viscoelastic properties

Complex viscosity and storage modulus were measured by means of a Physica MCR 501 rheometer from Anton Paar. Discs of 20 mm diameter and 2 mm width were obtained by injection molding in a HAAKE MiniJet Pro Injection System from Thermo Scientific using a cylinder temperature from 270 °C to 350 °C, molding temperature from 120 °C to 210 °C, injection pressure from 400 bar to 500 bar with a holding time of 6 s, and post pressure from 300 bar to 500 bar with a holding time of 2 s. A complete description of injection parameters for each blend is presented in the Supplementary Material Section. A parallel-plate geometry was used with a gap of 1 mm under a nitrogen atmosphere at a constant temperature of 280 °C. Strain sweeps were performed at different angular frequencies to define the linear viscoelastic region (LVR). Small amplitude oscillatory shear (SAOS) experiments were performed at 0.1% of amplitude in a scanning range from 300 rad/s to 0.1 rad/s. All specimens were vacuum dried at 110 °C during 16 h before LVR and SAOS tests to avoid the hydrolytic degradation of PBT.

### 2.4. Morphological analysis

Morphological evolution was studied using a scanning electron microscope SEM JOEL JSM-7100 and transmission electron microscope TEM Tecnai G2 F20 from FEI. SEM samples were immersed in liquid nitrogen for 20 min, mechanically cryofracture, and later coated with a gold layer. Selective dissolution of PEI phase was made by using the Soxhlet extraction technique. Samples were vacuum dry at 100 °C during 8 h to remove the excess of solvent. TEM samples were cut at room temperature in thin sections of approximately 60 nm thickness, using a Leica ultramicrotome coupled with a diamond knife. Image J software was used on SEM and TEM images processing to evaluate the shape of morphologies and particles size distribution. The number-average diameter ($Dn$) and volume-average diameter ($Dv$) are calculated using Equation (1) and Equation (2), and at least 100 particles were considered for this purpose.

$$Dn = \frac{\sum_i d_i}{n} \tag{1}$$

$$Dv = \left(\frac{\sum_i d_i^3}{n}\right)^{1/3} \tag{2}$$

### 2.5. Mechanical performance

Tensile tests were made according to ASTM D638 – 14 standard. Type V samples were injected molded in a HAAKE MiniJet Pro Injection System from Thermo Scientific using the same injection parameters as those previously described for DMA specimens. Samples were tested in an Instron 3366 at a crosshead speed of 1 mm/min using an extensometer with a gauge length of 10 mm. At least five specimens of each blend were measured and the average values were reported.

### 2.6. Thermal stability and flammability

Thermal stability of PEI, PBT, and PEI/PBT blends was studied in a TGA Q500 model from TA Instruments on samples of 40 QUOTE 2 mg, within a temperature range from 25 °C to 900 °C at a heating rate of 10 °C/min. All thermal evaluation tests were performed under nitrogen atmosphere.

Horizontal burning (HB) tests were performed according to the Underwriters Laboratories standard UL94 for “Plastic Materials for

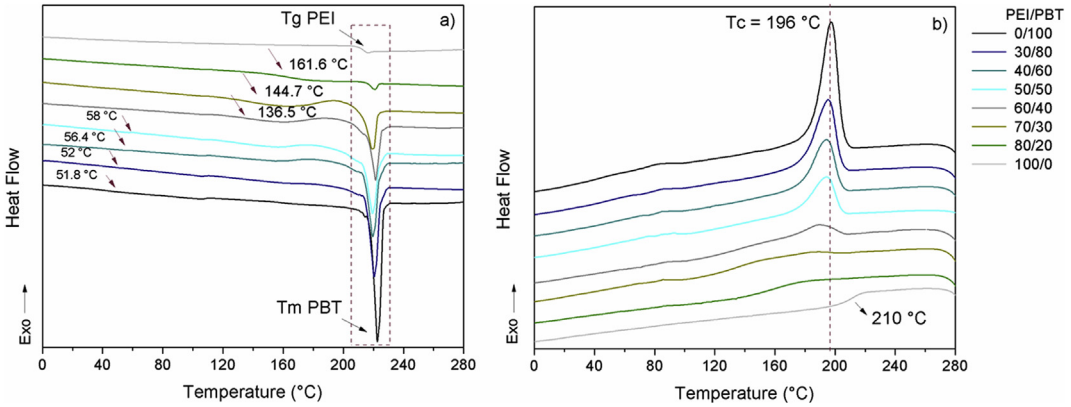


**Fig. 1.** Miscibility study of PEI/PBT blends from MDSC thermal analysis. Thermal transitions are presented during: a) the second heating on modulated mode (MDSC), and b) cooling. The data was reorganized on the y-axis.

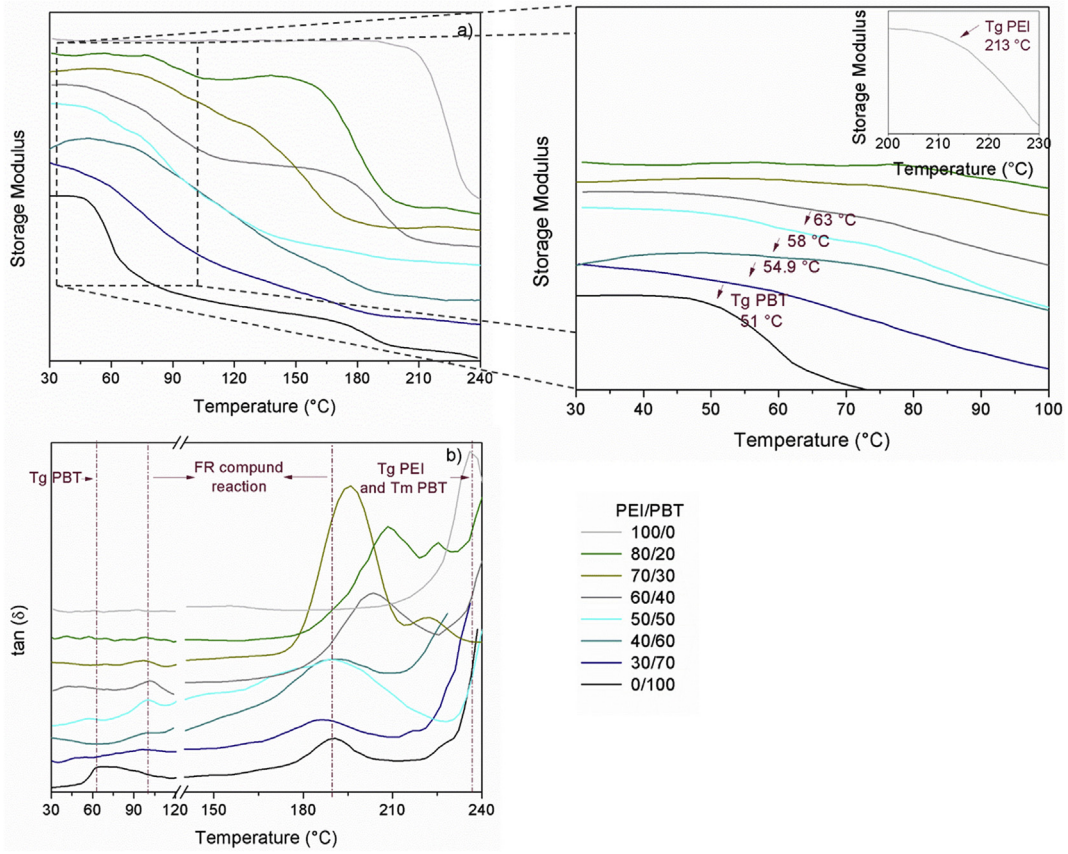


**Fig. 2.** Miscibility study of PEI/PBT blends from DMA analysis performed under torsional mode. It is presented: a) the storage modulus (G′) and b) tan (δ). The data was reorganized on the y-axis.

Parts in Devices and Appliances". Bars of 125 × 10 × 3 mm were obtained by injection molding in a HAAKE MiniJet Pro Injection System from Thermo Scientific using the same injection parameters as those previously described for DMA specimens, and at least three samples were tested for each blend. Flame traces in all samples were video and photographically recorded.

## 3. Results and discussion

### 3.1. Miscibility study

In Fig. 1, the MDSC results show that Tg of PEI (215.7 °C) and melting temperature (Tm) of PBT (222.5 °C) overlap in the range between 213 °C and 225 °C, hiding the Tg variation of PEI. Therefore, the following discussion will be focused on the Tg changes of PBT. Fig. 1a) shows that Tg of PBT shifts from 51.8 °C to 58 °C for PBT-rich blends, and that PEI-rich blends no longer exhibit thermal transition of PBT in this temperature range. The baseline variations for PEI-rich blends between 136 °C and 161 °C suggest that Tg of PBT shifts to higher temperatures as a sign of partial miscibility between both phases. The exothermic signal observed before the Tm of PBT in blends with 40, 50, 60, and 70 wt% of PEI, corresponds to Tcc of PBT. Tcc is characteristic of polymers that have passed through a quenching thermal treatment during cooling and appears at temperatures higher than Tg and lower than Tm [24]. When the quenched-in amorphous structure becomes mobile enough, crystallization occurs during heating

giving rise to an exothermic response. PEI/PBT blends in this work are cooled in air after the mixing process, and no thermal treatment is performed before DSC tests. However, PEI solidification takes place before that of PBT limiting its mobility and avoiding its crystallization, which leads to an "in-situ" quenching on PBT structure. Tcc is no longer observed in 80/20 blends as a sign of stronger molecular interaction between amorphous domains of PBT with PEI phase, and hence, of higher miscibility.

Fig. 1b) shows that the crystallization temperature (Tc) peak of PBT (196 °C) decreases with the increase of PEI concentration, being almost inhibited in 70/30 and 80/20 blends. The crystallinity of PBT phase —calculated from the melting peaks in Fig. 1a) using a 100% crystalline PBT with heat of fusion of 145 J/g [25]— is reduced from 18% for pure PBT, to 6% for 70/30 blend and 0.8% for 80/20 blend. This effect is caused by the segregation of PEI into the amorphous domain of PBT phase, which enriches the total amorphous domain of blends. Similar results were found in previous works on PEI/PBT blends [13]. However, authors reported Tc shifts to lower temperatures as a sign of miscibility. In our results, the dashed vertical line shows that Tc remains invariable. In contrast to other author's findings [13–17], PEI/PBT blends obtained under the experimental conditions used in this work are partially miscible at high PEI composition.

Fig. 2 shows the DMA results for pure PEI, PBT, and their blends. Tg values are calculated from the onset of the storage modulus G'. The thermal transitions of pure materials obtained by DMA are in good agreement with those from DSC results. In Fig. 2a), the G′ plot of PEI exhibits a sharp drop at 213 °C revealing its Tg. On the other hand, PBT displays a G' decline near 50 °C, corresponding to its Tg. In Fig. 2b), the tan (δ) plot shows that Tg of PEI and Tm of PBT overlap at 235 °C. Therefore, miscibility analyses from DMA results will be made in accordance with Tg of PBT.

The magnification on G' plot shows that Tg values of PBT, PBT-rich blends, and PEI are close to those obtained from DSC tests, and that PEI-rich blends do not show the Tg of PBT within the range between 51 °C and 63 °C. This confirms the "rejection" of the non-crystallizable segments on PBT from the emerging crystals, which acts as a diluent phase that enriches the amorphous phase of PEI/PBT blends [26]. As a result, PEI-rich blends tend to be miscible. Similar results are reported on PBT and bisphenol A poly(arylate) (PAr) blends [27,28] and PEEK and PEI blends [29,30].

In G' plot, the signal of PBT shows a second thermal transition at 180 °C undetected by MDSC analysis. According to EDS, XRD, Raman, and XPS results (shown in Supplementary Material Section), the flame retardant (FR) additive of PBT is a combination of bromides and antimony trioxide compounds. As reported by Rzyman and coworkers [31], bromides compounds melt in the range between 170 °C and 190 °C. The thermal transitions corresponding to the FR compound are evidenced in tan (δ) plots as a smooth peak at 100 °C and a peak at 188 °C. It is observed that both transitions remain constant for all PBT-rich blends.

Conversely, PEI-rich blends exhibit marked differences at temperatures higher than 180 °C. The signal of 60/40 blend shows a Tg shift caused by the partial miscibility between PEI and PBT phases. 70/30 blend reveals a strong signal produced by the overlapping of PBT cold crystallization, FR transition at 188 °C, and Tg of PEI. Finally, 80/20 blend shows a double-peak signal produced by the enrichment of amorphous domain in blends as a response of partial miscibility of PEI-rich blends.

### 3.2. Viscoelastic properties

Table 1 presents the results obtained at 280 °C and 300 rad/s for pure materials and their blends. As PBT has lower complex viscosity (η*) and lower storage modulus (G') than PEI, it improves the flow behavior of blends, even when small concentrations of PBT are added. As both, viscosity and storage modulus are temperature and frequency dependent, the viscosity ratio ($p = \eta_d/\eta_m$) and the elasticity ratio ($\psi = G'_d/G'_m$) —where $d$ corresponds to the dispersive phase and $m$ to the matrix— need to be calculated at the same processing conditions. Both $p$ and $\psi$ ratios values, exhibit a large difference when either PEI or PBT is the matrix. These differences in the viscoelastic properties have a direct effect on blends morphology, and will be discussed later on the morphological study results.

### 3.3. Morphology

#### 3.3.1. PBT-rich blends

In Fig. 3, there are displayed the SEM images with PEI selectively extraction (left) and the TEM micrographs (right) for three PBT-rich blends. The morphology of 10/90 blend shown in Fig. 3a), reveals that extraction of PEI phase leaves well-defined droplets of different sizes along the PBT matrix. The inserted image in SEM micrograph of Fig. 3a) displays a single PEI droplet before selective extraction, which is completely covered by a fibrillary matrix that corresponds to PBT phase. In SEM image, there are also noticed small undissolved spheres inside the former PEI domains. The TEM micrograph for the same blend shows the PBT matrix as a cloudy region because of its semicrystalline nature. The black spots correspond to antimony trioxide crystals, and the smoother and transparent regions to PEI droplets, with smaller cloudy-droplets inside. These results confirm that PEI droplets have PBT sub-inclusions due to a combination of two main effects: the steps processing method we used to fabricate the blends, and the significant differences in the viscoelastic properties between PEI and PBT previously described. At 280 °C, viscosity of PEI (5910 Pa.s) is much higher than that of PBT (299 Pa.s), leading to a high retention of PBT phase in PEI droplets. This phenomenon was described by Vanoene [32] and it was observed by Berger and coworkers in their experimental work with PET/PA blends [33]. Also, Favis and coworkers noticed composite droplets in PC/PP blends [34], and suggest that increasing the mixing time will diminished droplets retention. In our experiments, mixing times longer than 3 min will result in PBT thermal decomposition.

Phase distribution observed in PBT-rich blends seems to fit more to the classical theory of Taylor and Grace, which explains the effect of viscosity ratio on blends morphology. When highly viscous PEI is the dispersive phase, the viscosity ratio is greater than one ($p > > 1$), exceeding the breakup limit established by Taylor and Grace under shear deformation field ($p > 3.7$) [19,35] and preventing PEI droplets to deform and breakup into smaller particles. However, when the dispersive phase concentration increases the morphology formation is more influenced by the processing conditions. For instance, the PEI particles in 30/70 blends presented in Fig. 3b), have smaller size contrasted to those in 10/90 blends. This is due to higher concentrations of PEI are better homogenized by the kneaders during the mixing process, and hence, PEI particles in the 30/70 blends are elongated and broke up into finer particles. Additionally, as it is expected, higher concentrations of the dispersive phase enhance the number of particle-particle collisions and as a consequence, they coalesce. Fig. 3b) shows that PEI droplets in 30/70 blend are not as even and spherical as those observed in 10/90 blend. From TEM micrographs, it is confirmed that PEI particles coalesce when the concentration increases, giving as a result an uneven dispersive phase, with some droplets connected to each other. Several authors have studied the coalescence effect on the development of blends morphology [12,36–46], and they defined the basic influencing parameters during coalescence as: weight or volume fraction of dispersive phase, particle radius, phase's viscosity, and interfacial tension. They claim that high interfacial tensions lead to immiscibility between constituents and hence coalescence is enhanced.

So far, SEM results suggest that PEI and PBT are completely immiscible. However, the zoomed in image inserted in TEM micrograph of Fig. 3b), shows one PEI droplet in the 30/70 blend surrounded by well-defined spherulites of the semicrystalline PBT matrix that interpenetrate the PEI/PBT interface (dashed line). This phenomenon is known as inter-spherulitic interaction and is common in blends

**Table 1**
Viscoelastic properties of PEI/PBT blends, and viscosity ratios and storage modulus ratios for PBT-rich blends (PEI dispersed) and PEI-rich blends (PBT dispersed), calculated at 280 °C and 300 rad/s.

| Property | PEI/PBT blend | | | | | | | |
|---|---|---|---|---|---|---|---|---|
| | PBT | 30/70 | 40/60 | 50/50 | 60/40 | 70/30 | 80/20 | PEI |
| Complex viscosity (Pa.s) | 299 | 309 | 423 | 641 | 941 | 1090 | 1820 | 5910 |
| Storage modulus (Pa) | 29900 | 32100 | 62000 | 116000 | 186000 | 225000 | 422000 | 1690000 |
| | *PBT-rich blends* | | | | *PEI-rich blends* | | | |
| Viscosity ratio – $p$ | 19.77 | | | | 0.05 | | | |
| Storage modulus ratio – $\psi$ | 56.52 | | | | 0.02 | | | |

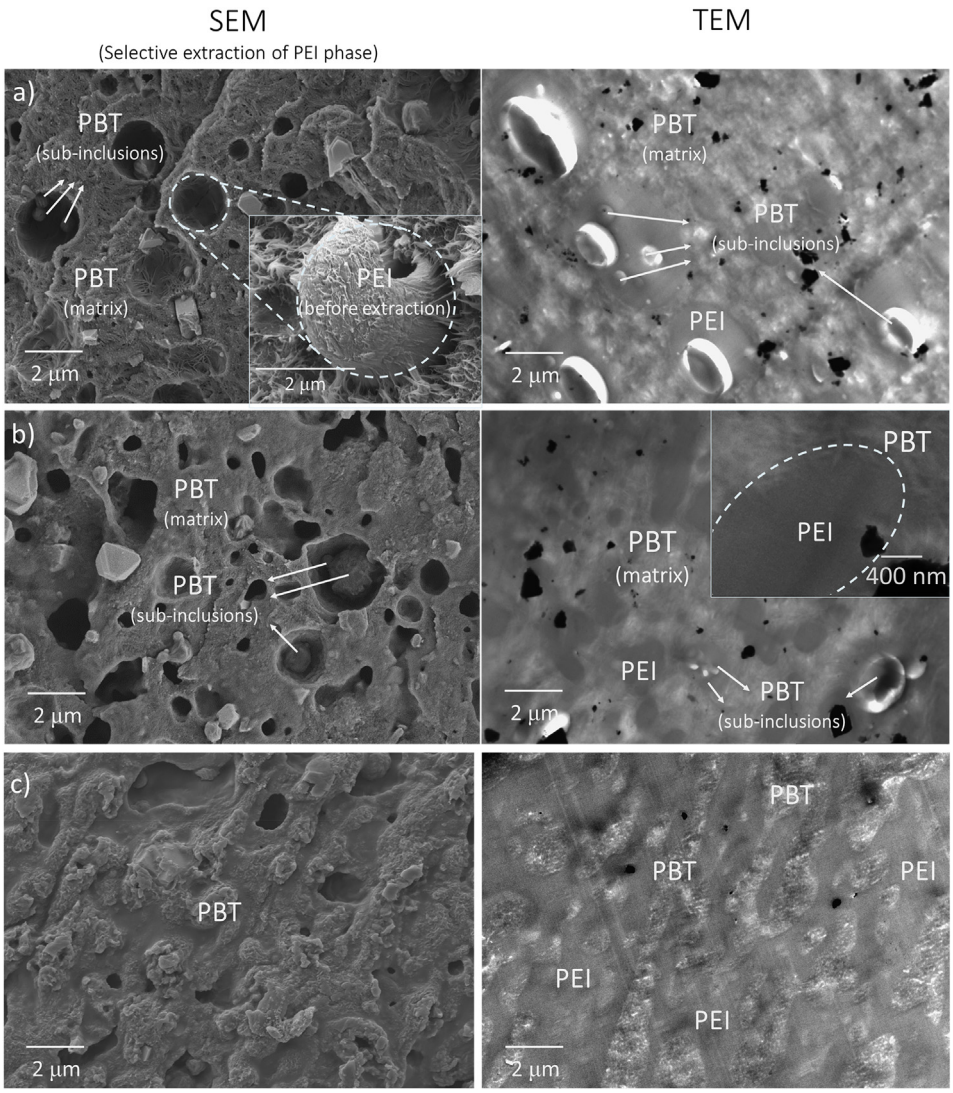


**Fig. 3.** Morphology of PBT-rich blends observed by SEM (left) and TEM (right), for PEI/PBT blends with: a) 10/90, b) 30/70, and c) 50/50. SEM micrographs show specimens with the extraction of PEI phase, and TEM micrographs show samples without PEI extraction.

between rigid amorphous and flexible semicrystalline polymers [26,47,48]. When PEI and PBT are mixed, PEI acts as an amorphous diluent of PBT amorphous phase, and some miscibility degree is achieved in the interface. This explains the smooth shifts of Tg observed for PBT-rich blends in MDSC between 51.8 °C and 58 °C range, and in DMA between 51 °C and 63 °C range.

In Fig. 3c), it is revealed that at even PEI and PBT concentrations it takes place a dual-phase transition event. In a complete compositional range study of immiscible polymers blend it is expected a phase inversion point, where the two phases are fully co-continuous and it is impossible to differentiate the matrix from the dispersive phase [49,50]. If the composition continues increasing the former matrix becomes the dispersed phase and the former dispersed phase becomes the matrix.

### 3.3.2. PEI-rich blends

Fig. 4 displays the morphology of blends after the phase transition. In Fig. 4a), the smoother appearance of PEI phase is more noticed due

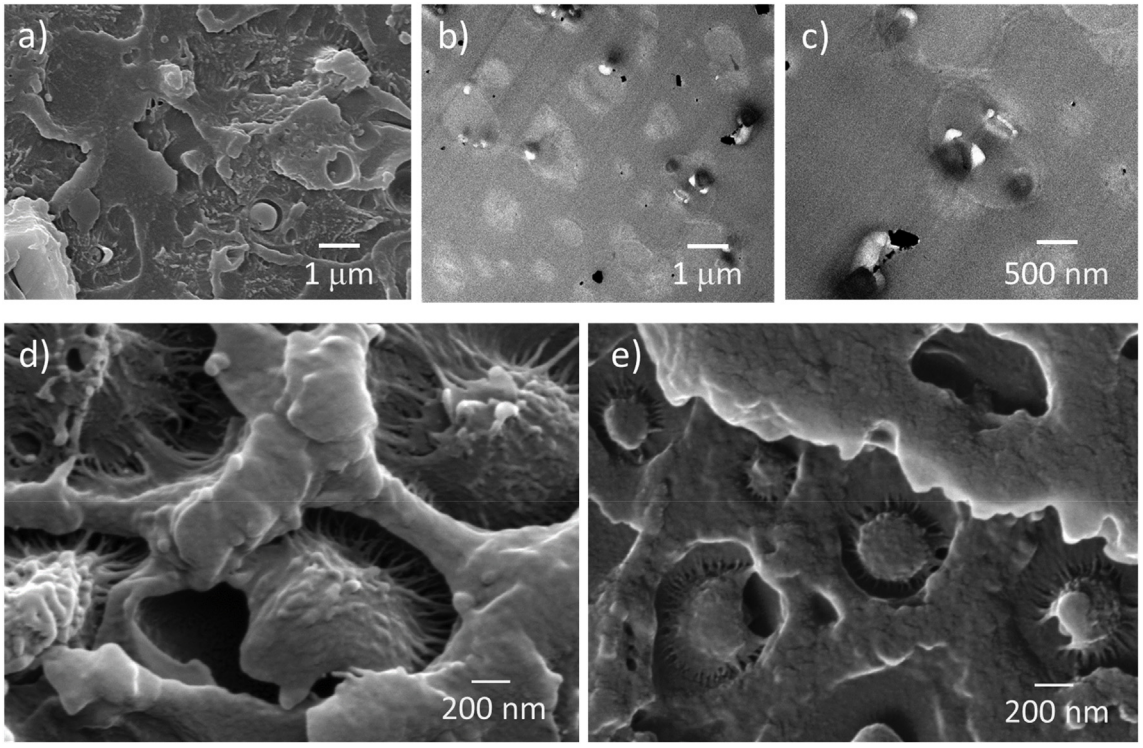


**Fig. 4.** Morphology of PEI-rich blends: a) SEM micrograph of 60/40 blend, b) and c) TEM micrographs of 60/40 blend, d) *spore-like* morphology of 70/30 blend, and e) *spore-like* morphology of 80/20 blend.

to the increase to 60 wt% of PEI, above the dual-phase inversion point, where it becomes the matrix and PBT the dispersive phase. The TEM micrograph shown in Fig. 4b), reveals that the PBT phase is distributed along the PEI matrix as droplets with irregular sizes and shapes —not as well defined as PEI droplets in PBT-rich blends—. A magnification presented in Fig. 4c), shows more in detail the fibrillary interface between PBT droplets adhered to the PEI matrix in 60/40 blends, which is found to be similar to the inter-spherulitic interaction previously described, suggesting that fibrillary interface is rich in PBT phase.

The increasing in PEI concentration leads to significant changes in PEI/PBT blends morphology. In Fig. 4d), it is noticed that small PBT droplets are attached to the PEI matrix with a more noticeable fibrillary interface, giving the appearance of what we call a *spore-like* morphology. In recent works, Bahrami and coworkers found that binary PPE/SAN blends compatibilized with SBM triblock terpolymer exhibit a similar morphology. They attributed the fibrillary linkage between PPE and SAN to the effect of the chemical compatibilization [51,52]. In our work, no compatibilizer agents are used and the interaction between PEI and PBT phases is a sign of good physical compatibilization between both phases. This singular morphology in PEI-rich blends is caused by the shrinkage differences between the two phases during the cooling stage after the two-step processing. Unlike the amorphous PEI phase, PBT is a semicrystalline polymer with fast crystallization rate, and a small shrinkage feature has been reported [53].

In their work in HDPE/PC blends, Leclair and Favis [54] explain that when an immiscible polymer blend is composed by a highly semicrystalline and a highly amorphous phase, a voiding mechanism takes place at the interface when the amorphous phase is the matrix. Immiscibility between HDPE and PC is attributed to their molecular structure differences, and to their transitions temperatures during cooling. In Fig. 5, it is presented a schematic representation of what happens to both PEI and PBT phases during the mixing process, as well as during the cooling stage after PEI-rich blends are removed from the mixer. When PBT is added to the fluid PEI (PEI is not semicrystalline and it does not melt) in step 2, PBT pellets melt, deform, and split into tiny droplets as a consequence of the shearing and elongation forces caused by the rotors speed and the highly viscous PEI phase. The cooling stage starts with both materials at 280 °C, with PEI fluid and PBT molten. At 210 °C, PEI phase is below its Tg and the matrix becomes rigid, hosting inside the still molten portion of immiscible PBT phase. When temperature reaches 196 °C, PBT starts to crystallize, and due to its semicrystalline nature, PBT droplets experience shrinkage leaving voids between both phases. However, these voids are combined with a fibrillary attachment between PBT droplets and the PEI matrix caused by the interspherulitic interaction between both phases, and hence, spore-like morphology is formed.

The previous morphological study suggests that PEI/PBT blends morphology strongly depends on the processing conditions, the viscoelastic differences between pure components, and PEI composition. In Fig. 6a), the dashed lines in the plot of average diameter vs. PEI concentration represent the generalized behavior of particles size before and after the phase inversion. It shows that particle size increases gradually with increasing composition as a consequence of coalescence, and just after phase inversion, the minor phase is deformed and breaks up into smaller particles [55–57]. The results for PEI/PBT blends presented in Fig. 6b), show that contrary to the generalized behavior, PEI droplets have coarser size at lower concentrations. This behavior is explained by the processing conditions proposed in this work, and the enormous differences between the viscoelastic properties of pure materials. When small concentrations of PEI (10 wt% of PEI) are added to the mixer during step 1, the kneaders soften and smoothly deform the PEI phase. When PBT phase is added during step 2, it melts and surrounds PEI phase, and as it is much less viscous than PEI, it distributes freely in the PBT matrix without suffering major deformation adopting coarse size droplets. When PEI concentration increases to 30 wt% and 40 wt%, a combination of shear and elongational flows takes place inside the mixer and PEI particles deform and break up into finer sizes. PEI-rich blends on the other hand, follow the generalized behavior. The increasing concentration of the highly viscous matrix leads to obtaining finer particles sizes of the less viscous dispersive phase.

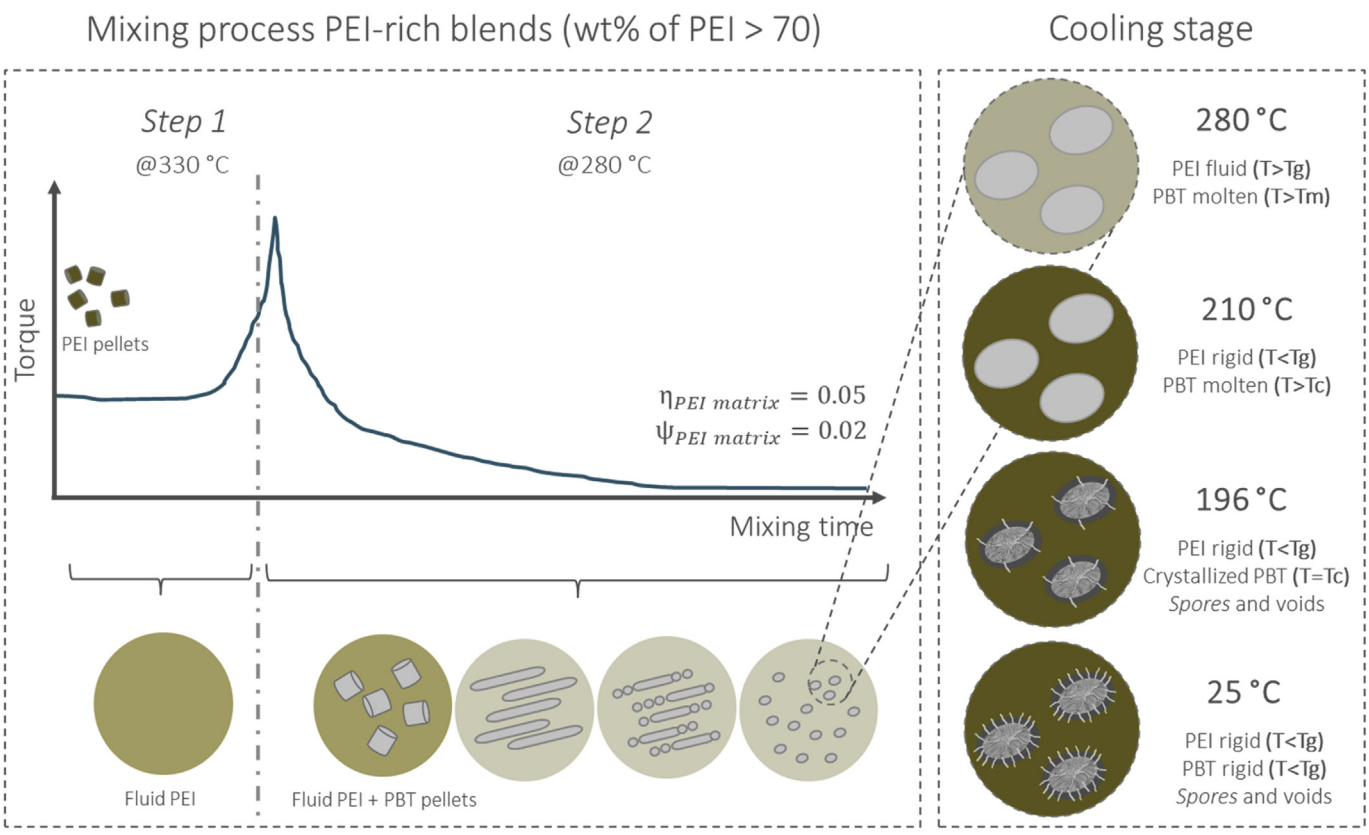


**Fig. 5.** Schematic representation of spore-like morphology formation in PEI-rich blends during their cooling stages.

In order to better observe the size and shape of the dispersive phase morphology when whether PBT or PEI is the matrix, Fig. 7 shows a schematic representation of PEI/PBT blends morphology evolution as a function of PEI composition. The scales of TEM micrographs for each blend are kept in their original size, and the drawn morphologies are modified to take all the particles to a common scale of 2 μm. The differences observed for each composition are entirely attributable to the processing parameters and to the mixing sequence used in this work. The interfacial tension —which strongly influences the morphology of immiscible blends— is considered to be constant for all blends compositions, since blending conditions in this work were kept constant for all PEI/PBT blends in the entire compositional range. According to Wu [58], interfacial tension between two substances will vary when there are changes in components polarities, temperature, and molecular weight of components. What does change for each blend while increasing PEI concentration is the morphology size and shape, and hence, the contact surface area between PEI and PBT. Contrary to other works on PEI/PBT blends, our results reveal that PEI and PBT phases are well differentiated from each other in the entire compositional range. The main differences with those reports are the characteristics of the commercial resins —we use flame retarded PBT—, the processing methods, and the step processing conditions.

### 3.4. Mechanical performance

#### 3.4.1. Tensile tests

Fig. 8 displays the stress vs. strain curves for pure materials and their blends. Pure PEI shows cold-drawing process after its yield stress

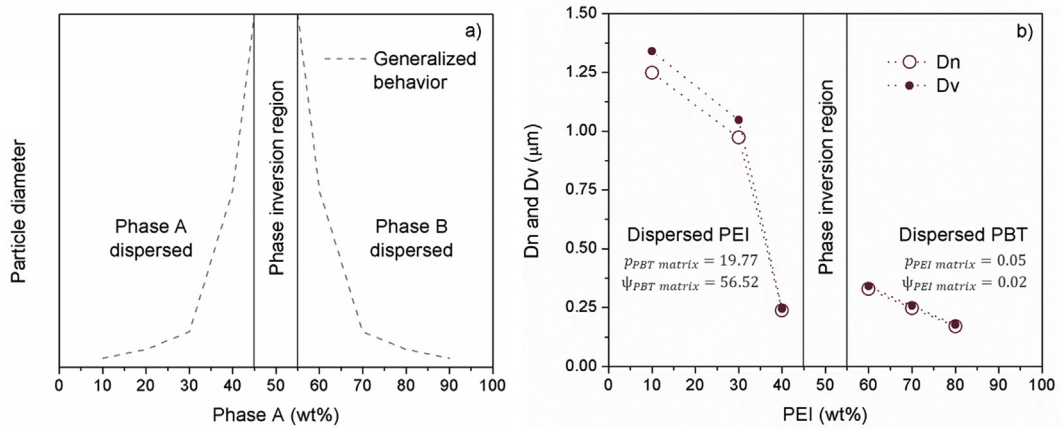


**Fig. 6.** Effect of blends composition on the size of the dispersive phase: a) Generalized behavior for blends with dual-phase inversion, and b) effect of PEI composition on the dispersed particle size of PEI/PBT blends.

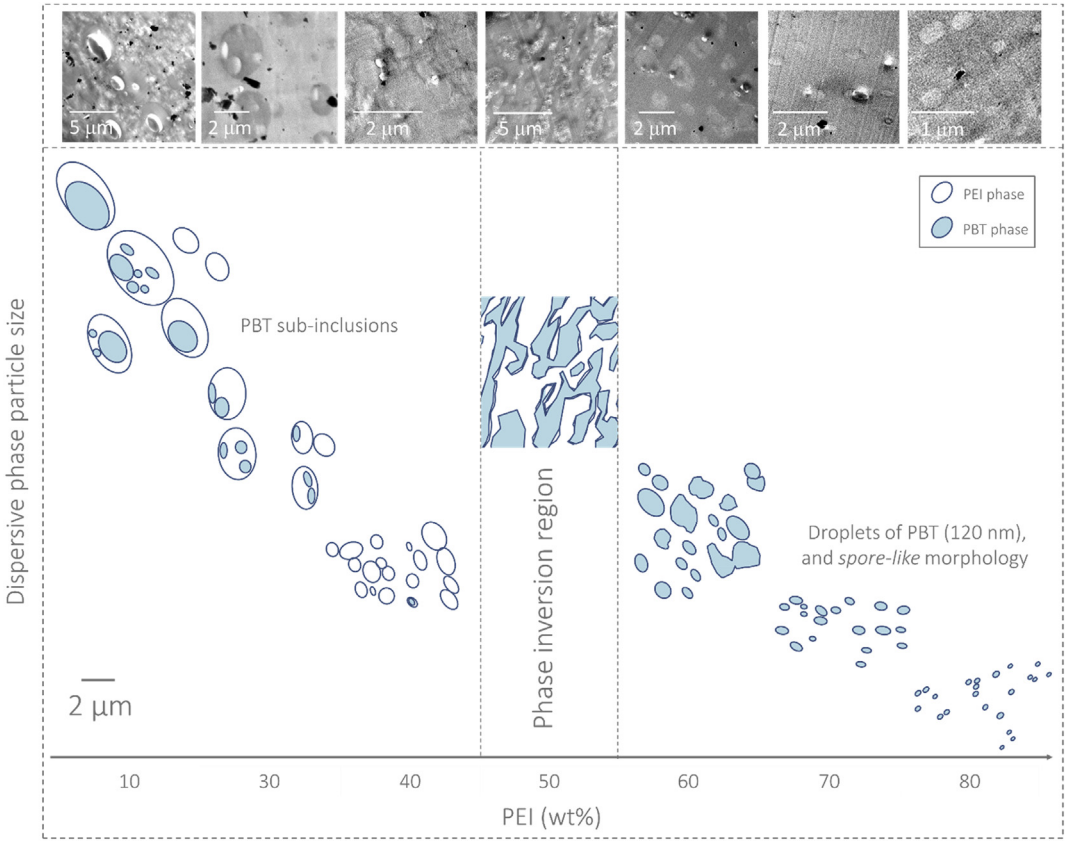


**Fig. 7.** Schematic representation of the morphological evolution of PEI/PBT blends in the entire compositional.

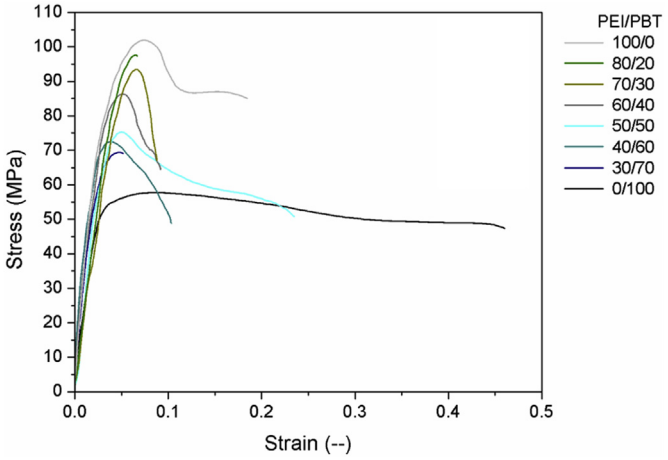


**Fig. 8.** Tensile stress-strain curves for PEI, PBT, and PEI/PBT blends.

($\sigma_y$), followed by a stress drop as a sign of necking. The stress stabilizes until PEI breaks at 20% deformation. PBT on the other hand, reaches its $\sigma_y$ and deforms gradually until it breaks after 40% deformation. Regarding PEI/PBT blends, they exhibit intermediate tensile strength with respect to pure components, which increases with PEI phase addition. However, there are clear differences in the elongational break performance of blends. Most blends exhibit cold-drawing behavior, but only 50/50 blend, and to some extent 40/60 and 60/40 blends, exhibit deformation similar to pure components. Two highly brittle blends are observed: 30/70 blend, and surprisingly 80/20 blend —with spore-like morphology— that break just after they reach the yield stress.

In Table 2 are listed the mechanical properties of PEI/PBT blends after tensile tests. The moduli values are calculated from the slope of the elastic region of stress-strain curves at early deformations where no interfacial debonding takes place [59,60]. It is noticed that all blends have intermediate values between those of pure constituents, which suggests that PEI and PBT phases are not incompatible in any composition.

**Table 2**
Mechanical performance of PEI/PBT blends.

| PEI/PBT blend | Modulus (MPa) | Tensile strength (MPa) | Ductility (%) |
|---|---|---|---|
| PBT | 1599.5 ± 298.7 | 56.9 ± 0.7 | 41.0 ± 6.4 |
| 30/70 | 1769.8 ± 278.5 | 67.6 ± 1.3 | 6.7 ± 1.0 |
| 40/60 | 2157.8 ± 463.3 | 71.9 ± 0.8 | 13.3 ± 5.2 |
| 50/50 | *2270.0 ± 258.7* | 74.7 ± 0.6 | 16.8 ± 4.0 |
| 60/40 | 2095.1 ± 230.9 | 83.6 ± 1.7 | 11.1 ± 3.2 |
| 70/30 | 2028.9 ± 245.2 | 91.6 ± 1.1 | 13.5 ± 3.9 |
| 80/20 | *2515.5 ± 519.6* | 96.9 ± 1.9 | 6.1 ± 1.3 |
| PEI | 2267.8 ± 257.4 | 103.6 ± 1.5 | 26.6 ± 10.4 |

The low modulus value of 30/70 and 70/30 blends, is explained from the morphology exhibited in SEM and TEM results. Blends with 30 wt% of PEI have a coarse PEI particles size together with PBT sub-inclusions that lead to low mechanical performance. Additionally, PBT-rich blends have higher amount of FR filler, which acts as stress concentrations leading to poorer mechanical performance. Blends with 70 wt% on the other hand, shows that spores are formed leaving large spaces between PBT domains and the PEI matrix (Fig. 4d)). These voids promote the early fracture of blends.

Blends containing 40 wt% and 60 wt% of PEI display higher moduli values, due to their proximity to the phase inversion region (co-continuous morphology). This is in good agreement with the inter-spherulitic interaction between PEI and PBT phases, which enhance the interfacial bonding through the fibrillary structure.

The blends with 50 wt% and 80 wt% of PEI, exhibit a synergetic

contribution (values presented in italics in Table 2) associated with the form in which phases are distributed. In 50/50 blends, PEI and PBT are co-continuous and the contribution of the highly rigid PEI phase is noticed as a substantial increase in modulus values. The synergic behavior observed in the blend containing 80 wt% of PEI is a combination of the higher concentration of PEI in the blend, the distribution of the crystalline PBT phase in the shape of tiny spores-like structure, and the rigidity gained by the densification caused by the inter-spherulitic interaction. Vallejo and coworkers reported similar synergic results for PEI-rich blends [16], and it is explained from a thermodynamic approach that explains the free volume effect on the mechanical properties of polymer blends [61,62]. When an exothermic reaction occurs during blends' components interaction, Gibbs free energy of mixing is negative and the blend will be miscible. What should be expected then, is a volume contraction in the blend known as densification. This phenomenon known as "thermal embrittlement" explains the embrittlement that occurs when miscible blends with high Tg polymers —such as PEI— experiences free volume loss. As discussed previously, PEI-rich blends exhibit partial miscibility that favors the free volume loss and hence, densification of the blends. This behavior leads blends to exhibit higher moduli than those of pure materials, and as a consequence, synergism is observed.

The $\sigma_y$ of PEI/PBT blends is calculated as the maximum stress in the elastic-to-plastic transition region. Contrary to the elastic modulus, the yield stress in polymer blends is sensitive to adhesion of components, and generally indicates if the interface is strong enough to transmit the tensile stress up to break [59,60]. Similarly to moduli, it is observed that $\sigma_y$ values increase monotonically with PEI addition. In their study, Leclair and Favis observed that when semicrystalline and amorphous polymers are blended, it is reached a reinforcement effect when the amorphous phase is added to the semicrystalline matrix. They obtained HDPE/PC blends in the entire compositional range, and noticed the mentioned effect when PC is added to HDPE. Conversely, when HDPE is added to the PC matrix, no adhesion is observed at the interface and the mechanical performance decreased for PC-rich blends [54]. At difference of Leclair and Favis results, we noticed an interface reinforcement in PBT-rich blends with the interspherulitic formation, and in PEI-rich blends with the spore-like morphology.

Surprising results are observed in the ductility behavior. For all blends, ductility is lower than that of pure components. This is explained from blends morphological structure and partial miscibility. PBT-rich blends are immiscible, with coarse PEI domains, sub-inclusions of PBT in PEI droplets, and with inorganic fillers (FR compoinds) which causes stresses concentration and promotes early fracture. On the other hand, PEI-rich blends are partially miscible, and their poor elongation at break is attributable to the thermal embrittlement, resulting in a considerable increase in modulus or strength together with a dramatic reduction in ductility [61,63]. Nevertheless, it is noticed that ductility of the blend with 50 wt% of PEI is the highest due to its co-continuous morphology.

### 3.5. Thermal stability and flammability

#### 3.5.1. Thermal stability

In Fig. 9 are presented the results from the thermogravimetric analysis for pure components and their blends. It is noticed that PEI exhibits higher thermal stability than flame retarded PBT. In addition, PEI has an inherent charring ability [64], which is noticed by the mass loss value lower than 50%. The decomposition of pure materials takes place in a single step, which is retained in the corresponding blends leading to an intermediate two-step decomposition behavior. The small signal observed at 500 °C in pure PBT —enclosed in the orange dashed circle— corresponds to the oxidation of one of the components of the flame retardant additive: $Sb_2O_3$ [65–67]. When $Sb_2O_3$ starts to oxidize, it reacts with the bromide compound to produce an antimony-bromide complex that acts with a synergistic effect delaying the flame propagation —just in case the polymer undergoes a combustion process—, as described by Sallet and coworkers in their work [68].

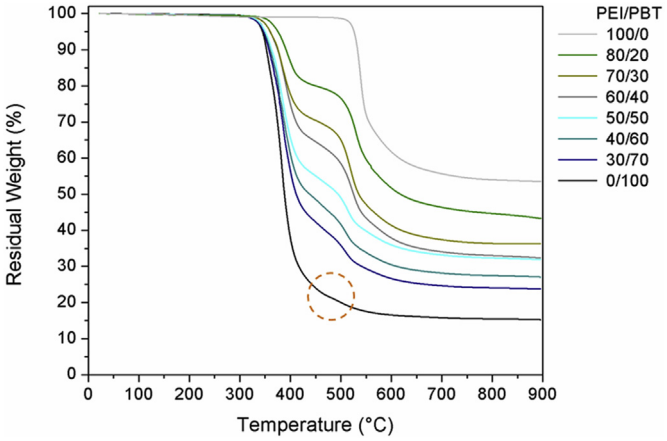


**Fig. 9.** Thermal stability of PEI, PBT, and PEI/PBT blends by TGA.

TGA results reveal that PEI/PBT blends decomposition is strongly influenced by each polymer thermal behavior. However, it is not clear the existence of possible interactions between blends' constituents or their decomposition products. Several authors have reported that depending on the nature of these interactions blends may exhibit positive or negative effects on thermal stability [69–74]. Although it is not the aim of this work to study the mechanisms of decomposition of PEI/PBT blends, we calculated the theoretical TGA curves by using the additivity relation that allows studying the interaction between PEI, PBT, and their decomposition products. If the experimental data of the individual components is multiplied by a factor corresponding to the wt% of each component in the blend, the resulting data will represent the thermal behavior expected for each composition in the absence of any kind of interaction between phases or their decomposition products [69–73]. The differences found between both, the experimental and calculated data, yields information about the existence of some kind of interaction that could involve diffusion of small species (molecule-molecule, molecule-radical, radical-radical) [69].

In Fig. 10, there are presented the experimental and calculated results of three PEI/PBT blends containing 30 wt%, 50 wt% and 80 wt% of PEI. The curves for pure polymers are also shown for comparative purposes. The solid lines represent the behavior observed experimentally and the dashed lines the calculated weight loss curves in the

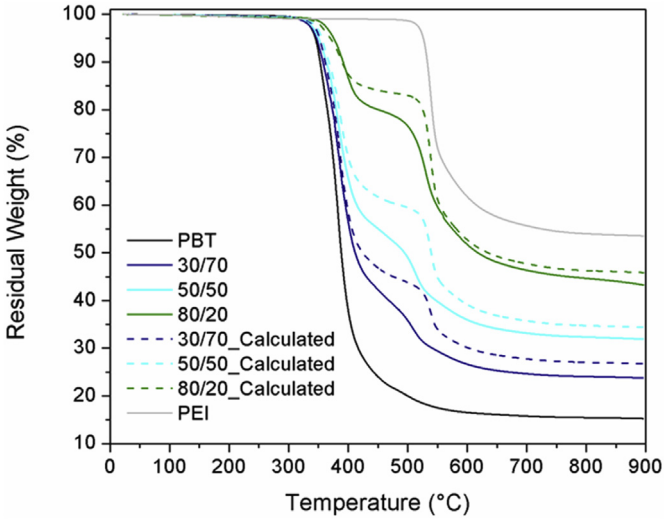


**Fig. 10.** Experimental and calculated TGA curves for three representative PEI/PBT blends: 30/70, 50/50 and 80/20.

absence of any interaction. For all compositions, it is noticed that both curves have a similar tendency, with two-step decomposition behavior corresponding to each phase response. During the first decomposition step the experimental and predicted curves are in good agreement. PEI delays the initial degradation of PBT phase improving its thermal stability. In their work on PVC/PS blends, Dodson and coworkers [70] found that the TGA signal for blends containing 1:1 by weight of each component exhibited a notorious delay in the weight loss curve within the range between 250 °C and 350 °C. In this region, the initial decomposition of PVC takes place, hence the delay is attributable to PS phase help to retard the dehydrochlorination reaction of PVC. Nevertheless, our results reveal clear differences between experimental and calculated curves that appear just before the decomposition signal of the second step. It is noticed that the loss weight behavior of the experimental curves is lower than that of the theoretical curves, as a sign of some kind of interaction that is taking place, leading to the less stable polymer (PBT) destabilize the more stable one (PEI). Some PBT thermal decomposition products or byproducts (butadiene, tetrahydrofuran, or acetaldehyde) [75–77] may interact with the PEI molecule causing its prompt degradation during step two.

The presence of the flame retardant additive in the blends (antimony trioxide and bromide compounds) also affects the thermal stability of PEI. In the morphological analysis of blends, it is observed that $Sb_2O_3$ particles are well dispersed along the whole samples, even in the PEI phase of PEI-rich blends. The decomposition event observed at 500 °C —which correspond to antimony oxide signal— coincide with the early decomposition of the PEI phase in the blends, accelerating the presence of decomposition products such as phenol, benzonitrile, and isopropylene groups that commonly appear at 550 °C [78]. This effect is more noticed in the blend containing 50 wt% of PEI, where both phases have a co-continuous phase distribution.

### 3.5.2. Flammability

Fig. 11 presents the results for all blends after 4 min of direct flame exposure. The upper dashed line delimits the maximum length of the specimens (125 mm), and the lower dashed line the first mark at a length of 25 mm from the specimen's tip. It is noticed that in neither, the pure polymers nor their blends, the flame reach the first mark located at 25 mm from specimen's tip after 60 s exposure. We expose the samples to flame more than 60 s, and no significant burning rate evolution was observed. These results indicate PEI/PBT blends classify as slow burning specimens (HB) according to UL94 standard for horizontal burning tests. Materials classified under this test should not have or exceed a burning rate of 75 mm/min over a 75 mm distance, for specimen's thickness of 3 mm. Burning rate of PEI/PBT blends is much lower than that stablished by the standard of 75 mm/min.

As observed in TGA results, the decomposition of PBT does not lead to high carbonaceous residues production (charring formation). However, for PBT flammability results show that flame do not reach the 25 mm mark after 120 s of direct flame exposure, suggesting that PBT flame retardancy is controlled by the synergic self-extinguish effect caused by the antimony oxides and bromide compound reaction [68,79–81]. This assumption is made on the basis that the carbonaceous products formed over PBT surface are not large enough to avoid flame propagation and material consumption. Conversely, results for blends suggest that the flame retardancy is dominated by a combination of the self-extinguish effect of PBT additive with a strong influence of PEI charring formation. Large amounts of charring products are formed over the specimens avoiding flame propagation through the inner sample. Finally, a remarkable flame resistance of PEI sample is observed. The flame does not propagate along the PEI specimen because of the layer of charring products formed. Even after 4 min of direct flame contact, the PEI sample integrity remains almost intact.

## 4. Conclusions

For the first time, it is reported a complete miscibility and morphological study in melt processed PEI/PBT blends together with their viscoelastic, mechanical, thermal, and flammability performance evaluation. Results from miscibility study revealed that PEI/PBT blends are partially miscible and strongly dependent on PEI composition, and two groups of blends were identified as PBT-rich blends and PEI-rich blends. PBT-rich blends resulted being immiscible with coarse PEI particles distributed along the PBT matrix, together with little sub-inclusions of PBT retained by the highly viscous PEI phase. PEI-rich blends on the other hand, exhibited partial miscibility with tiny PBT droplets well dispersed along the PEI matrix giving as a result a new morphology called spore-like morphology. Additionally, we found that at even concentrations of PEI and PBT blends experience a phase transition where PEI and PBT phases are co-continuous.

Since the mechanical, thermal, and flammability performance is clearly influenced by miscibility of PEI/PBT blends, it is possible controlling blends morphology in order to tailor their properties for specific high-performance applications. For instance, PBT-rich blends exhibited the lowest tensile strength and poor ductility due to the coarse PEI droplets size; but at the same time the best melt processability which is evidenced in their low viscosity and storage modulus values. PEI-rich blends on the other hand, revealed the highest tensile properties and a synergetic contribution on Young modulus in 80/20 blend is noticed. Although the ductility of these group of blends is also compromised by blends densification, they have better processability than pure PEI. On the other hand, 50/50 blend also exhibits synergetic contribution on tensile modulus and the highest ductility of all blends due to its co-continous morphology. Regarding the thermal and flammability performance, the addition of PEI increases the thermal stability of PBT phase and reduces the flame propagation rate in PEI/PBT blends promoting charring formation as the main flame retardant mechanism.

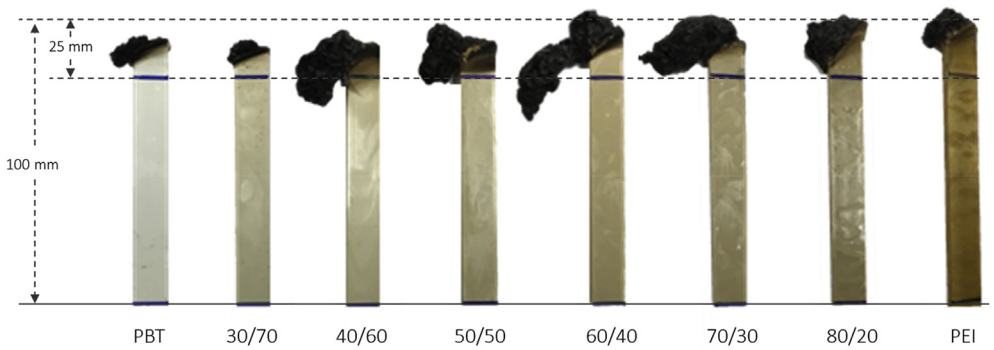


**Fig. 11.** Photographs of the specimens of pure PEI, pure PBT, and PEI/PBT blends, after 4 min in direct contact with the flame in the HB test. PEI content increasing is shown from left to right.

## Acknowledgements

Authors like to thank the financial support from Universidad Eafit. Mauricio Vásquez would like to thank Colciencias for the Ph.D. scholarship. For this work, the facilities of the Cornell Center for Materials Research Shared supported through Prof. Juan P. Hinestroza, and the facilities of École de technologie supérieure supported through Prof. Nicole Demarquette were used. Also, thanks to Natalia de Fátima Sánchez-Arrieta who contributed to the chemical analysis of PEI/PBT blends.

## Appendix A. Supplementary data

Supplementary data related to this article can be found at https://doi.org/10.1016/j.polymer.2018.09.012.

## References

[1] P. Bajaj, Fire-retardant materials, Bull. Mater. Sci. 15 (1992) 67–76.
[2] L.A. Utracki, Characterization methods for high temperature polymer blends, High Temp. Polym. Blends, Elsevier, 2014, pp. 14–69.
[3] J.E. Mark, Polymer Data Handbook, Oxford University Press, Cincinnati, 2008.
[4] M.T. DeMeuse, High temperature polymer blends: an overview of the literature, Polym. Adv. Technol. 6 (1995) 76–82.
[5] M. Jaffe, P. Chen, E.-W. Choe, T.-S. Chung, S. Makhija, High performance polymer blends, in: P.M. Hergenrother (Ed.), High Perform. Polym, Springer-Verlag, Berlin/Heidelberg, 1994, pp. 297–327.
[6] L.A. Utracki, Polymer Blends Handbook, Kluwer, Dordrecht, 2002.
[7] B.D. Favis, D. Therrien, Factors influencing structure formation and phase size in an immiscible polymer blend of polycarbonate and polypropylene prepared by twin-screw extrusion, Polymer 32 (1991) 1474–1481, https://doi.org/10.1016/0032-3861(91)90429-M.
[8] Z. Shi, L. Utracki, Development of polymer blend morphology during compounding in a twin-screw extruder. Part II: theoretical derivations, Polym. Eng. Sci. 32 (2004) 1834–1845.
[9] J.K. Lee, C.D. Han, Evolution of polymer blend morphology during compounding in a twin-screw extruder, Polymer 41 (2000) 1799–1815.
[10] H. Potente, M. Bastian, A. Gehring, M. Stephan, P. Pötschke, Experimental investigation of the morphology development of polyblends in corotating twin-screw extruders, J. Appl. Polym. Sci. 76 (2000) 708–721.
[11] M. Polaskova, R. Cermak, T. Sedlacek, J. Kalus, M. Obadal, P. Saha, Extrusion of polyethylene/polypropylene blends with microfibrillar-phase morphology, Polym. Compos. 31 (2009) 1427–1433, https://doi.org/10.1002/pc.20928.
[12] H. Li, U. Sundararaj, Morphology development of polymer blends in extruder: the effects of compatibilization and rotation rate, Macromol. Chem. Phys. 210 (2009) 852–863, https://doi.org/10.1002/macp.200800543.
[13] J. Jang, K. Sim, Crystallization behavior in poly (ether imide)/poly (butylene terephthalate) blends using a spectroscopic method, Polym. Test. 17 (1998) 507–521, https://doi.org/10.1016/S0142-9418(97)00066-4.
[14] E.M. Woo, S.N. Yau, Peculiar glass transition behavior and miscibility in a binary mixture comprising amorphous poly (ether imide) with semicrystalline poly (butylene terephthalate), Macromolecules 30 (1997) 3626–3631, https://doi.org/10.1021/ma961031a.
[15] H.-L. Chen, J.C. Hwang, C.-C. Chen, R.-C. Wang, D.-M. Fang, M.-J. Tsai, Phase behaviour of amorphous and semicrystalline blends of poly(butylene terephthalate) and poly(ether imide), Polymer 38 (1997) 2747–2752, https://doi.org/10.1016/S0032-3861(97)85610-8.
[16] F.J. Vallejo, J.I. Eguiazábal, J. Nazábal, Solid state features and mechanical properties of PEI/PBT blends, J. Appl. Polym. Sci. 80 (2001) 885–892, https://doi.org/10.1002/1097-4628(20010509)80:6<885::AID-APP1166>3.0.CO;2-D.
[17] E.M. Woo, S.N. Yau, Two-stage crystallization kinetics modeling of a miscible blend system containing crystallizable poly (butylene terephthalate), Polym. Eng. Sci. 38 (1998) 583–589, https://doi.org/10.1002/pen.10221.
[18] M. Vásquez-Rendón, N. Sánchez-Arrieta, M. Álvarez-Láinez, Two-step processing method for blending high-performance polymers with notable thermal and rheological differences: PEI and PBT, Polym. Plast. Technol. Eng. (2017), https://doi.org/10.1080/03602559.2017.1381256 null-null.
[19] C. Harrats, S. Thomas, G. Groeninckx (Eds.), Micro- and Nanostructured Multiphase Polymer Blend Systems: Phase Morphology and Interfaces, Taylor & Francis, Boca Raton, Fla, 2006.
[20] D.R. Paul, J.W. Barlow, Polymer blends, J. Macromol. Sci. Part C. 18 (1980) 109–168, https://doi.org/10.1080/00222358008080917.
[21] L.A. Utracki, C.A. Wilkie (Eds.), Polymer Blends Handbook, Springer Netherlands, Dordrecht, 2014, , https://doi.org/10.1007/978-94-007-6064-6.
[22] S. Mazinani, S. Darvishmanesh, R. Ramazani, B. Van der Bruggen, Miscibility of polyimide blends: physicochemical characterization of two high performance polyimide polymers, React. Funct. Polym. 111 (2017) 88–101, https://doi.org/10.1016/j.reactfunctpolym.2016.12.010.
[23] Z. Ma, G. Zhang, Q. Yang, X. Shi, J. Li, H. Zhang, J. Qin, Tailored morphologies and properties of high-performance microcellular poly(phenylene sulfide)/poly(ether ether ketone) (PPS/PEEK) blends, J. Supercrit. Fluids 140 (2018) 116–128, https://doi.org/10.1016/j.supflu.2018.06.010.
[24] B. Wunderlich, Theory of cold crystallization of high polymers, J. Chem. Phys. 29 (1958) 1395–1404, https://doi.org/10.1063/1.1744729.
[25] R.L. Blaine, Thermal Applications Notes: Polymers Heats of Fusion, (n.d.).
[26] D.S. Kalika, Viscoelastic characterizatiion of polymer blends, in: D.R. Paul, C.B. Bucknall (Eds.), Polym. Blends Vol. 1 Formul, John Wiley & Sons, Inc., NY, USA, 2000.
[27] J. Runt, D.M. Miley, K.P. Gallagher, X. Zhang, C.A. Barron, S.K. Kumar, Poly (butylene terephthalate)–polyarylate blends, Polym. Adv. Technol. 5 (1994) 333–338.
[28] J.P. Runt, X. Zhang, D.M. Miley, K.P. Gallagher, A. Zhang, Phase behavior of poly (butylene terephthalate)/polyarylate blends, Macromolecules 25 (1992) 3902–3905.
[29] J.F. Bristow, D.S. Kalika, Investigation of semicrystalline morphology in poly (ether ether ketone)/poly (ether imide) blends by dielectric relaxation spectroscopy, Polymer 38 (1997) 287–295.
[30] R.H. Mehta, D.A. Madsen, D.S. Kalika, Microporous membranes based on poly (ether ether ketone) via thermally-induced phase separation, J. Membr. Sci. 107 (1995) 93–106.
[31] M. Rzyman, M. Grabda, S. Oleszek-Kudlak, E. Shibata, T. Nakamura, Studies on bromination and evaporation of antimony oxide during thermal treatment of tetrabromobisphenol A (TBBPA), J. Anal. Appl. Pyrolysis 88 (2010) 14–21, https://doi.org/10.1016/j.jaap.2010.02.004.
[32] H. Vanoene, Modes of dispersion of viscoelastic fluids in flow, J. Colloid Interface Sci. 40 (1972) 448–467.
[33] W. Berger, H.W. Kammer, C. Kummerlöwe, Melt rheology and morphology of polymer blends, Macromol. Chem. Phys. 8 (1984) 101–108.
[34] B.D. Favis, C. Lavallee, A. Derdouri, Preparation of composite dispersed phase morphologies in incompatible and compatible blends during melt processing, J. Mater. Sci. 27 (1992) 4211–4218.
[35] B.D. Favis, Factors influencing the morphology of immiscible polymer blends in melt processing, in: D.R. Paul, C.B. Bucknall (Eds.), Polym. Blends Vol. 1 Formul, John Wiley & Sons, Inc., NY, USA, 2000.
[36] V. Everaert, L. Aerts, G. Groeninckx, Phase morphology development in immiscible PP/(PS/PPE) blends influence of the melt-viscosity ratio and blend composition, Polymer 40 (1999) 6627–6644, https://doi.org/10.1016/S0032-3861(99)00048-8.
[37] B.D. Favis, The effect of processing parameters on the morphology of an immiscible binary blend, J. Appl. Polym. Sci. 39 (1990) 285–300.
[38] I. Fortelný, L.I. Minkova, J. Kotek, M. Lapčíková, D. Michálková, Morphology and mechanical properties of polypropylene/polystyrene blends compatibilized with styrene-butadiene block copolymers, Polym. Eng. Sci. 52 (2012) 191–204, https://doi.org/10.1002/pen.22066.
[39] R. Gonzalez-Nunez, B.D. Favis, P.J. Carreau, C. Lavallee, Factors influencing the formation of elongated morphologies in immiscible polymer blends during melt processing, Polym. Eng. Sci. 33 (1993) 851–859.
[40] Y. Li, S. Hu, J. Sheng, Evolution of phase dimensions and interfacial morphology of polypropylene/polystyrene compatibilized blends during mixing, Eur. Polym. J. 43 (2007) 561–572, https://doi.org/10.1016/j.eurpolymj.2006.10.018.
[41] C.W. Macosko, Morphology development and control in inmiscible polymer blends, Macromol. Symp. 149 (2000) 171–184.
[42] N. Tokita, Analysis of morphology formation in elastomer blends, Rubber Chem. Technol. 50 (1977) 292–300.
[43] S. Ravati, B.D. Favis, Morphological states for a ternary polymer blend demonstrating complete wetting, Polymer 51 (2010) 4547–4561, https://doi.org/10.1016/j.polymer.2010.07.014.
[44] P. Van Puyvelde, S. Velankar, J. Mewis, P. Moldenaers, K.U. Leuven, Effect of Marangoni stresses on the deformation and coalescence in compatibilized immiscible polymer blends, Polym. Eng. Sci. 42 (2002) 1956–1964.
[45] C.E. Scott, C.W. Macosko, Processing and morphology of polystyrene/ethylene-propylene rubber reactive and nonreactive blends, Polym. Eng. Sci. 35 (1995) 1938–1948.
[46] P.K.S. Mural, M.S. Rana, G. Madras, S. Bose, PE/PEO blends compatibilized by PE brush immobilized on MWNTs: improved interfacial and structural properties, RSC Adv. 4 (2014) 16250–16259, https://doi.org/10.1039/C4RA01961J.
[47] S.D. Hudson, D.D. Davis, A.J. Lovinger, Semicrystalline morphology of poly (aryl ether ether ketone)/poly (ether imide) blends, Macromolecules 25 (1992) 1759–1765.
[48] B.S. Hsiao, B.B. Sauer, Glass transition, crystallization, and morphology relationships in miscible poly (aryl ether ketones) and poly (ether imide) blends, J. Polym. Sci., Part B: Polym. Phys. 31 (1993) 901–915.
[49] P. Pötschke, D.R. Paul, Formation of Co-continuous structures in melt-mixed immiscible polymer blends, J. Macromol. Sci. Polym. Rev. 43 (2003) 87–141, https://doi.org/10.1081/MC-120018022.
[50] F. Prochazka, R. Dima, J.-C. Majesté, C. Carrot, Phase inversion and co-continuity domain in immiscible polyethylene/polystyrene blends, E-Polymers 3 (2003) 512–522.
[51] R. Bahrami, T.I. Löbling, H. Schmalz, A.H.E. Müller, V. Altstädt, Synergistic effects of Janus particles and triblock terpolymers on toughness of immiscible polymer blends, Polymer 109 (2017) 229–237, https://doi.org/10.1016/j.polymer.2016.12.044.
[52] R. Bahrami, T.I. Löbling, H. Schmalz, A.H.E. Müller, V. Altstädt, Micromechanics of “raspberry” morphology in PPE/SAN polymer blends compatibilized with linear ABC triblock terpolymers, Polymer 80 (2015) 52–63, https://doi.org/10.1016/j.polymer.2015.10.039.
[53] I. Phillin, S. Pimbert, J.-F. Feller, G. Levesque, Crystallization kinetics of poly(butylene terephthalate) (PBT): influence of additives and free carboxylic acid chain

ends, Polym. Eng. Sci. 41 (2001) 178–191, https://doi.org/10.1002/pen.10720.
[54] A. Leclair, B.D. Favis, The role of interfacial contact in immiscible binary polymer blends and its influence on mechanical properties, Polymer 37 (1996) 4723–4728.
[55] D. Bourry, B.D. Favis, Cocontinuity and phase inversion in HDPE/PS blends: influence of interfacial modification and elasticity, J. Polym. Sci., Part B: Polym. Phys. 36 (1998) 1889–1899.
[56] S. Joseph, M. Rutkowska, M. Jastrzêbska, H. Janik, J.T. Haponiuk, S. Thomas, Polystyrene/polybutadiene blends: an analysis of the phase-inversion region and cophase continuity and a comparison with theoretical predictions, J. Appl. Polym. Sci. 89 (2003) 1007–1016.
[57] S.V. Nair, Z. Oommen, S. Thomas, Phase morphology development and melt rheological behavior in nylon 6/polystyrene blends, J. Appl. Polym. Sci. 86 (2002) 3537–3555, https://doi.org/10.1002/app.11159.
[58] S. Wu, Interfacial and surface tensions of polymer melts and liquids, Polym. Interface Adhes, Marcel Dekker, Inc., New York, 1982, pp. 67–132.
[59] J. Kolařk, Simultaneous prediction of the modulus, tensile strength and gas permeability of binary polymer blends, Eur. Polym. J. 34 (1998) 585–590.
[60] K.P. Tchomakov, B.D. Favis, M.A. Huneault, M.F. Champagne, F. Tofan, Mechanical properties and morphology of ternary PP/EPDM/PE blends, Can. J. Chem. Eng. 83 (2005) 300–309.
[61] J.W. Barlow, D.R. Paul, Polymer blends and alloys—a review of selected considerations, Polym. Eng. Sci. 21 (1981) 985–996.
[62] M.C. Schwarz, J.W. Barlow, D.R. Paul, Mechanical properties of HDPE/(PEC/PS)/SEBS blends, J. Appl. Polym. Sci. 35 (1988) 2053–2067.
[63] E.A. Joseph, M.D. Lorenz, J.W. Barlow, D.R. Paul, Mechanical properties of miscible polycarbonate-copolyester blends, Polymer 23 (1982) 112–122.
[64] S. Carroccio, C. Puglisi, G. Montaudo, Thermal degradation mechanisms of polyetherimide investigated by direct pyrolysis mass spectrometry, Macromol. Chem. Phys. 200 (1999) 2345–2355.
[65] N. Li, Y. Xia, Z. Mao, L. Wang, Y. Guan, A. Zheng, Influence of antimony oxide on flammability of polypropylene/intumescent flame retardant system, Polym. Degrad. Stabil. 97 (2012) 1737–1744, https://doi.org/10.1016/j.polymdegradstab.2012.06.011.
[66] R.G. Orman, D. Holland, Thermal phase transitions in antimony (III) oxides, J. Solid State Chem. 180 (2007) 2587–2596, https://doi.org/10.1016/j.jssc.2007.07.004.
[67] R.G. Orman, Phase Transitions in Antimony Oxides and Related Glasses, University of Warwick, 2005.
[68] D. Sallet, V. Mailhos-Lefievre, B. Martel, Flame retardancy of polyamide 11 with a decabromodiphenyl-antimony trioxide mixture. A bromine-antimony-nitrogen synergism, Polym. Degrad. Stabil. 30 (1990) 29–39.
[69] I. Campoy, M.A. Gómez, C. Marco, Thermogravimetric analysis of blends based on nylon 6 and a thermotropic liquid crystal copolyester, J. Therm. Anal. 52 (1998) 705–715.
[70] B. Dodson, I.C. McNeill, Degradation of polymer mixtures. VI. Blends of poly (vinyl chloride) with polystyrene, J. Polym. Sci. Polym. Chem. Ed. 14 (1976) 353–364.
[71] I.C. McNeill, J.G. Gorman, S. Basan, Thermal degradation of blends of PVC with poly (tetramethylene sebacate), Polym. Degrad. Stabil. 33 (1991) 263–276.
[72] M. Naffakh, G. Ellis, M.A. Gómez, C. Marco, Thermal decomposition of technological polymer blends 1. Poly(aryl ether ether ketone) with a thermotropic liquid crystalline polymer, Polym. Degrad. Stabil. 66 (1999) 405–413.
[73] I. Ray, S. Roy, D. Khastgir, Interaction between ethylene vinyl acetate copolymer and polyethylene, Polym. Bull. 30 (1993) 685–689.
[74] F.P. La Mantia, M. Morreale, L. Botta, M.C. Mistretta, M. Ceraulo, R. Scaffaro, Degradation of polymer blends: a brief review, Polym. Degrad. Stabil. 145 (2017) 79–92, https://doi.org/10.1016/j.polymdegradstab.2017.07.011.
[75] K.C. Khemani, A novel approach for studying the thermal degradation, and for estimating the rate of acetaldehyde generation by the chain scission mechanism in ethylene glycol based polyesters and copolyesters, Polym. Degrad. Stabil. 67 (2000) 91–99.
[76] R. Kinoshita, Y. Teramoto, H. Yoshida, TG-DTA/FT-IR method for analyzing thermal decomposition mechanism of polyesters, J. Therm. Anal. 40 (1993) 605–611.
[77] G. Montaudo, Primary Thermal Degradation Mechanisms of PET and PBT, (n.d.).
[78] L.H. Perng, Thermal degradation mechanism of poly(ether imide) by stepwise Py–GC/MS, J. Appl. Polym. Sci. 79 (2000) 1151–1161.
[79] F. Montezin, J.-M. Lopez-Cuesta, A. Crespy, P. Georlette, Flame retardant and mechanical properties of a compolymer PP/PE containing brominated compounds/antimony trioxid blends and magnesium hydrixide or talc, Fire Mater. 21 (1997) 245–252.
[80] M. Półka, J. Gałaj, Z. Karpovič, Investigation into the influence of flame retardant additives on some fire properties of polyester materials applying small-scale testing techniques, J. Civ. Eng. Manag. 19 (2013) 561–572, https://doi.org/10.3846/13923730.2013.793610.
[81] H. Sato, K. Kondo, S. Tsuge, H. Ohtani, N. Sato, Mechanisms of thermal degradation of a polyester flame-retarded with antimony oxide/brominated polycarbonate studied by temperature-programmed analytical pyrolysis, Polym. Degrad. Stabil. 62 (1998) 41–48.